JACS
JOURNAL OF THE AMERICAN CHEMICAL SOCIETY
Article
pubs.acs.org/JACS

Singlet Fission in a Covalently Linked Cofacial Alkynyltetracene Dimer

Nadezhda V. Korovina,[‡] Saptaparna Das,[‡] Zachary Nett, Xintian Feng, Jimmy Joy, Ralf Haiges, Anna I. Krylov, Stephen E. Bradforth,* and Mark E. Thompson*

Department of Chemistry, University of Southern California, Los Angeles, California 90089, United States

Supporting Information

ABSTRACT: Singlet fission is a process in which a singlet exciton converts into two triplet excitons. To investigate this phenomenon, we synthesized two covalently linked 5-ethynyltetracene (ET) dimers with differing degrees of intertetracene overlap: BET-X, with large, cofacial overlap of tetracene π-orbitals, and BET-B, with twisted arrangement between tetracenes exhibits less overlap between the tetracene π-orbitals. The two compounds were crystallographically characterized and studied by absorption and emission spectroscopy in solution, in PMMA and neat thin films. The results show that singlet fission occurs within 1 ps in an amorphous thin film of BET-B with high efficiency (triplet yield: 154%). In solution and the PMMA matrix the S_1 of BET-B relaxes to a correlated triplet pair $^1(T_1T_1)$ on a time scale of 2 ps, which decays to the ground state without forming separated triplets, suggesting that triplet energy transfer from $^1(T_1T_1)$ to a nearby chromophore is essential for producing free triplets. In support of this hypothesis, selective excitation of BET-B doped into a thin film of diphenyltetracene (DPT) leads to formation of the $^1(T_1T_1)$ state of BET-B, followed by generation of both DPT and BET-B triplets. For the structurally cofacial BET-X, an intermediate forms in <180 fs and returns to the ground state more rapidly than BET-B. First-principles calculations predict a 2 orders of magnitude faster rate of singlet fission to the $^1(T_1T_1)$ state in BET-B relative to that of crystalline tetracene, attributing the rate increase to greater coupling between the S_1 and $^1(T_1T_1)$ states and favorable energetics for formation of the separated triplets.

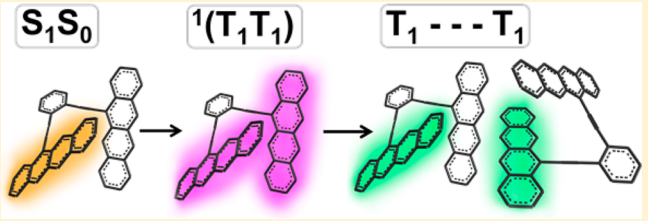

INTRODUCTION

Singlet fission is a process in which a chromophore, excited to its singlet excited state, interacts with an adjacent chromophore to form two triplets. The triplets produced by singlet fission can subsequently diffuse away from each other and be independently harvested in a photovoltaic device. Thus, this process has the potential to double the photocurrent in solar cells at wavelengths where the singlet fission is operational. The power conversion efficiency of a single junction photovoltaic cell is limited to 33%.[1] Incorporation of materials capable of undergoing singlet fission into a photovoltaic device raises the upper limit of the power conversion efficiency of a single junction device to 45%.[2]

The singlet fission process is illustrated in Figure 1. The singlet excited state rapidly forms a correlated pair of triplets with an overall singlet character, $^1(T_1T_1)$, followed by its dissociation into two separated triplets.[2] In this paper we use the term singlet fission to refer to the formation of $^1(T_1T_1)$, distinguishing this step from the two triplets diffusing apart. While many researchers have investigated singlet fission,[3−8] the complete mechanistic picture remains elusive. There are three basic requirements for singlet fission to lead to "free" triplets: (1) the energy of the singlet state of a given material has to be close to twice that of the triplet state, (2) the rate of singlet fission must be faster than the rates of other excited-state relaxation pathways, and (3) the triplets must be able to dissociate from the correlated triplet pair.

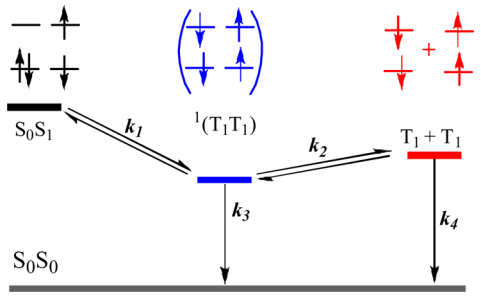

Figure 1. Schematic representation of the singlet fission process.

Little is known about the correlated pair, $^1(T_1T_1)$, since this intermediate state is rarely observed directly.[9−11] Based on the model presented in Figure 1, the rate of formation of the $^1(T_1T_1)$ state is controlled by two factors: the energy difference between the states involved, and the electronic couplings between the states. The rate of separation of the two triplets from the $^1(T_1T_1)$ state depends on the energies and couplings

Received: October 17, 2015
Published: December 22, 2015

DOI: 10.1021/jacs.5b10550
J. Am. Chem. Soc. 2016, 138, 617−627

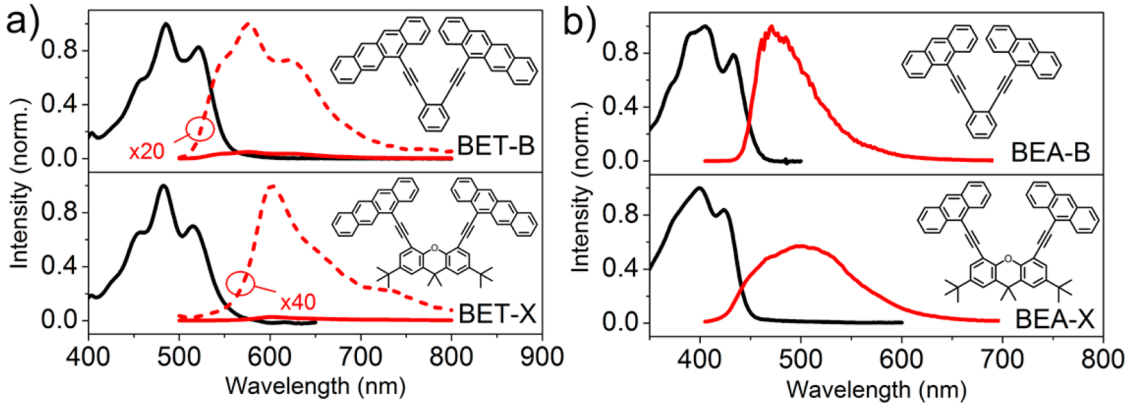

Figure 2. Comparison of absorption (black) and emission (red) spectra of the (a) tetracene dimers versus the (b) anthracene dimers in a PMMA matrix. The areas of the emission peaks for BET-X, BET-B and BEA-X are normalized to a BEA-B area of 1.0. The photoluminescence efficiencies for BEA-X and BEA-B are 57% and 96%, respectively.

between the states of interest and can also be enhanced by an increase in entropy upon separation.[12,13]

The energy requirement for singlet fission is fulfilled in polyacenes of four rings (tetracene) and greater.[6,11,14] In contrast to pentacene whose singlet fission is strongly exergonic, singlet fission in tetracene derivatives is slightly endergonic. Having S_1 and $2 \times T_1$ energies being close reduces energetic losses upon singlet fission and can lead to improved open-circuit voltage in photovoltaic devices. This also provides the means for understanding the entropic contributions in triplet generation via singlet fission. Certain biradicaloid materials, such as isobenzofuran derivatives, have also been shown to satisfy this energetic requirement,[5] and efforts are being made to develop new singlet fission materials with a biradicaloid electronic structure.[15,16] Acenes and diphenylisobenzofuran have demonstrated singlet fission with near unit efficiency (triplet yield = 200%) in crystalline and polycrystalline samples.[3,5,8,17]

Previous work published by our groups has shown that 5,12-diphenyltetracene (DPT) undergoes efficient singlet fission in amorphous thin films (triplet yield = 122%).[14] The kinetics of singlet fission in this material show a fast exponential (~1 ps) triplet rise followed by a slower power law rise of the triplet population spread over hundreds of picoseconds. The two phases are associated with direct and diffusive singlet fission processes, respectively. The direct process originates from excitation on or adjacent to the sites with DPT molecules arranged in a preferred orientation for singlet fission, whereas the diffusive phase arises when migration of a singlet exciton is required from the excitation site to the preferred fission site. It has been predicted that the fast singlet fission sites have two DPT molecules in a preferred dimer arrangement; however, there are <5% of such dimer sites present in the amorphous films.[14] Nevertheless, the singlet fission rate at the preferred DPT sites is markedly faster than those reported for tetracene polycrystalline thin films (9–90 ps) and single crystals (40–300 ps).[6,8,14,18–21] Thus, it is desirable to have every pair of molecules in a thin film arranged in the preferred orientation for fast singlet fission, to eliminate the slower diffusive singlet fission, since the diffusion process is a potential source of the exciton loss. Ideally singlet fission should outcompete other (loss) processes.

An important question is which relative chromophore orientation(s) will maximize the coupling between S_0S_1 and $^1(T_1T_1)$ states and thus promote singlet fission in a chromophore dimer?[22] Michl et al. have suggested that a slipped cofacial orientation maximizes the coupling matrix element,[2,15] while a recent theoretical study has found that the largest coupling and the fastest singlet fission rate corresponds to the in-plane arrangement of the chromophores in diphenylisobenzofuran crystals.[23] Importantly, relative orientation of the chromophores also affects the key energetic parameters and can control other excited-state relaxation pathways. For instance, formation of excimers[24] or charge-transfer states[25] can proceed rapidly, on a time scale similar to that of singlet fission. The role of excimers in the singlet fission mechanism is uncertain. According to several studies of substituted pentacenes, the excimer state is a doorway to the $^1(T_1T_1)$ state.[11,26–28] In tetracene-based systems, so far only one study reports triplet formation from an excimer.[10]

Several dimers have been studied, with the goal of finding an optimal orientation for singlet fission. Solution measurements give a triplet yield of 3% for linearly linked tetracene dimers,[29,30] and a yield of 9% for linearly linked dimers of isobenzofuran.[31] Pentacene dimers, in which singlet fission is significantly exoergic, and donor–acceptor thiophene-based polymers have been observed to undergo "unimolecular" singlet fission in solution.[32–35] Co-facial bis-perylene-diimide[36,37] and tetracene[38] dimers have been observed to relax to the ground state via an excimer state.

In this work we investigate the photophysics of two cofacial ethynyl-tetracene dimers, BET-B and BET-X (Figure 2). In BET-X the overlap of the tetracenes is large, while in the BET-B the intertetracene overlap is markedly smaller (but greater than in previously studied covalent dimers[29]). It was observed that the amount of π overlap has a large impact on the excited-state dynamics of the dimers, such that BET-X relaxes to the ground state very rapidly, possibly via an excimer or $^1(T_1T_1)$ state, while BET-B yields a long-lived $^1(T_1T_1)$ state on a picosecond time scale. Additionally, separated triplets, as well as the $^1(T_1T_1)$ state of BET-B, have been observed in the solid state, which allowed us to gain insight into the mechanism of separation of triplets from the correlated triplet pair.

To preview the role that the geometric configuration imposed on the pairs of tetracenes by the xanthene and benzene cores plays in the photophysics of these dimers, we compare the ethynyltetracene (ET) dimers (BET-B and BET-X) to their ethynylanthracene (EA) analogs (BEA-B and BEA-X) (Figure 2). The energy requirements for singlet fission $[E(S_1) \geq 2E(T_1)]$ are met for the tetracene-based dimers, but

DOI: 10.1021/jacs.5b10550
J. Am. Chem. Soc. 2016, 138, 617–627

not for their anthracene-based analogs. The EA dimers exhibit high emission intensities when suspended in a rigid poly(methyl methacrylate) (PMMA) matrix (57% for BEA-X, and 96% for BEA-B). The emission intensity of the tetracene analogs, on the other hand, is strongly quenched in the same media (2.6% for BET-X, and 5.0% for BET-B). This suggests that the lower $E(T_1)/E(S_1)$ ratio in BET-B and BET-X opens an additional channel of excited state deactivation, presumably singlet fission, which is energetically inaccessible in BEA-B and BEA-X.

EXPERIMENTAL SECTION

General. The synthesis and characterization of all of the materials studied here and the details of the sample preparation are given in the Supporting Information. UV−visible spectra were recorded on a Hewlett-Packard 4853 diode array spectrophotometer. The steady-state emission at room temperature and 77 K was measured with Photon Technology International QuantaMaster QM-400 spectrofluorometer. Fluorescence lifetimes at 77 K were determined by the time-correlated single-photon counting (TCSPC) technique, using IBH Fluorocube with a 405 nm LED excitation source, and an IRF value of 0.4 ns. TCSPC of the neat films at room temperature were measured using 500 nm excitation (Coherent RegA, 250 kHz) with a fast R3809U-50 photomultiplier tube (time resolution ∼22 ps).

Femtosecond Transient Absorption. The apparatus has been described previously.[14] In brief, pump and probe pulses were derived from the output of a Ti:sapphire regenerative amplifier (Coherent Legend, 1 kHz, 4 mJ, 35 fs). Excitation pulses centered at either 500 or 550 nm were generated using a type-II OPA (Spectra Physics OPA-800C). White light supercontinuum probe pulses, spanning the visible (320−950 nm) were obtained by focusing a small amount of the amplifier output into a rotating CaF_2 disk. To avoid any orientational contribution to the observed dynamics,[39] the polarization of the supercontinuum probe was set at the magic angle (54.7°) with respect to the pump polarization. The probe was collimated and focused with a pair of off-axis parabolic mirrors into the sample whereas the pump pulse was focused using a CaF_2 lens. The cross correlation between the pump and probe in a quartz substrate matched to that used to support films had an fwhm of 150 fs averaged across the probe spectrum for 500 nm excitation. A slightly longer instrument response of 170 fs was found for 550 nm excitation. The instrument response for the solution measurements is slightly higher, at 180 fs. The supercontinuum probe was dispersed using a spectrograph (Oriel MS127I) onto a 256-pixel silicon diode array (Hamamatsu). Spectra were measured for a range of excitation fluences from 12 to 96 $\mu J/cm^2$ for ET-TMS thin film and 8 to 64 $\mu J/cm^2$ for BET-B thin film. The TA data shown in Figure 5 are reported at 24 $\mu J/cm^2$ and 16 $\mu J/cm^2$ for ET-TMS and BET-B, respectively. The solution measurements were performed with a pump fluence of ∼25 $\mu J/cm^2$. Samples were slowly translated perpendicular to the path of the pump and probe using a linear stage to prevent photodamage.

Computational Details. Computational methods that were used to estimate the relative rates of singlet fission in the tetracene dimers are presented here. The molecular geometries were computed by starting with the experimentally obtained crystal structures (one structure for BET-B and two for BET-X, given below), fixing the positions of the heavy atoms, and allowing the C−H bonds to relax. The structures of excimers were optimized by following the lowest-excited singlet state in the TDDFT calculations. ωB97X-D/cc-pVDZ was used in all optimizations. The degrees of overlap between the frontier orbitals of tetracenes in BET-X_1, BET-X_2, BET-B, and a tetracene dimer in a herringbone orientation from the crystal structure of tetracene were computed using Q-Chem[31] as follows. First, Hartree−Fock wave functions of the individual tetracene moieties in a field of the polarizable point charges of the rest of the system were computed. The MOs from these fragment calculations were then used to evaluate the overlap integrals between the HOMOs and LUMOs of the tetracene moieties.[40] The electronic couplings between the relevant states, excitation energies, and rates were calculated using a previously reported protocol,[13,23,41] based on the RAS-2SF wave functions.[42−44] The couplings between the adiabatic states were quantified by the norm of the transition density matrix (denoted by $\|\gamma\|$) connecting the interacting states (the magnitude of coupling is proportional to $(\|\gamma\|/\Delta E)$, where ΔE is the energy difference between the respective RAS-CI states).[41] Energies, couplings, and rates were computed for BET-B, BET-X_1, BET-X_2, and a pair of tetracenes in a herringbone orientation, and two excimer structures. The rates of singlet fission in the dimers were calculated using the Fermi Golden Rule and a free energy relationship:[13]

$$k_1[S_0S_1 \rightarrow {}^1(T_1T_1)] \approx \left(\frac{\|\gamma\|}{\Delta E}\right)^2 e^{-\alpha\beta E_{sf}} \quad (1)$$

$$k_2[{}^1(T_1T_1) \rightarrow 2T_1] \approx e^{-\alpha\beta E_b} \quad (2)$$

where E_{sf} denotes the energy drive for singlet fission defined as $E_{sf} = E({}^1(T_1T_1)) - E(S_1)$ and E_b is the multiexciton stabilization energy defined as $E_b = E({}^5(T_1T_1)) - E({}^1(T_1T_1))$, β is $1/k_BT$, and α comes from a linear free energy analysis (we used $\alpha = 0.5$ as in previous studies).[13,41] We note that the absolute excitation energies are hard to calculate reliably. As explained previously,[13] we use empirical energy additivity correction to account for missing dynamical correlation effects. Our scheme also benefits from the built-in error cancellation, since it relies on energy differences between homologically similar compounds (note that the correction cancels out exactly in relative rate calculations). The success of this protocol for computing the relative rates in various compounds provides empirical validation of this computational scheme.[13,23]

RESULTS

We prepared two different dimers of ET to examine how the relative orientations of the two chromophore units affect singlet fission and other photophysical processes in these systems. The synthesis of the dimers was carried out analogously to that of similar dimers reported in the literature.[38,45] First, 5-ethynyltetracene (ET) was prepared by bromination of tetracene to give 5-bromotetracene, followed by Sonogashira coupling with TMS-acetylene to give ET-TMS, and finally hydrolysis of the TMS group to give ET. BET-X and BET-B were formed by Sonogashira coupling of ET with the appropriate dihaloarene, i.e., 4,5-dibromoxanthene and 1,2-diiodobenzene, respectively (Supporting Information (SI), Scheme S1).

Crystal Structures of BET-B and BET-X. The tetracene moieties in BET-B are oriented at ∼20° angle with respect to each other, as illustrated in Figure 3a. This molecule belongs to the C_2 point group, with approximately one ring worth of overlap between the tetracenes (Figure 3a). The distance between the tetracenes within BET-B ranges from 3.1 to 3.8 Å, as indicated in Figure 3b. The intermolecular packing of BET-B in the crystal places tetracenes from neighboring molecules in a slip-stacked arrangement (along the long and the short axes) with a π-facing orientation (see SI, Figure S7). The intermolecular tetracene distance in crystalline BET-B is 3.4 Å.

The asymmetric unit of BET-X has two structurally distinct forms, shown in Figure 3c and 3d. The acenes of one BET-X dimer, BET-X_1 (Figure 3c), are slanted at a 50° angle relative to the xanthene core resulting in a slip-stacked geometry with three acene rings overlapping. In the other BET-X dimer, BET-X_2 (Figure 3d), the acenes are nearly perpendicular to the xanthene core, with all four rings overlapping. In both of the BET-X dimers the distance between the tetracenes is 3.4−3.5 Å. In crystals of BET-X, all intermolecular pairs of tetracenes are perpendicularly oriented, and no intermolecular tetracene−

DOI: 10.1021/jacs.5b10550
J. Am. Chem. Soc. 2016, 138, 617−627

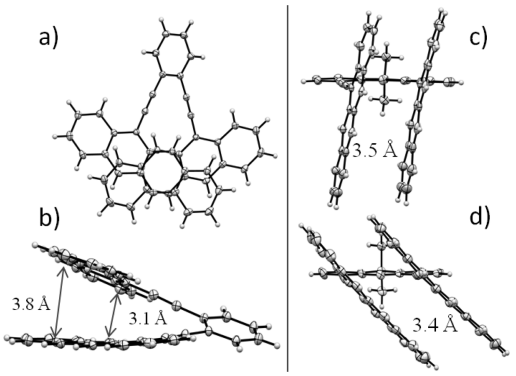

Figure 3. (a and b) Crystal structure of BET-B, (c) crystal structure BET-X_1 (intertetracene spacing = 3.4 Å), and (d) crystal structure BET-X_2 (intertetracene spacing = 3.5 Å). The view chosen here has the xanthene moiety of the BET-X structures perpendicular to the page, with the *tert*-butyl groups removed for clarity.

tetracene $\pi-\pi$ packing is observed (see SI, Figure S8). In an amorphous film, however, intermolecular π overlap of the tetracenes is certainly possible.

The intermolecular distances in substituted tetracene crystals, such as diphenyltetracene, dithiophenyltetracene, and rubrene range from 3.2 to 3.8 Å.[22,46−49] The intramolecular tetracene distances in our dimers and the intermolecular tetracene distance in BET-B are similar to those between the tetracenes in other substituted tetracene crystals.

Theoretical Modeling of Singlet Fission in Ethynyltetracenes. The degree of overlap between tetracene moieties in each dimer is expected to impact the coupling and thus the excited-state dynamics. The tetracene overlap in the dimers and for a dimer pair in the tetracene crystal was quantified by the overlap between frontier MOs (HOMOs and LUMOs) of the two tetracenes. The HOMO overlaps in BET-X_1 and BET-X_2 are 3.4% and 2.8% respectively. As expected, the overlaps calculated for both BET-B and the herringbone tetracene dimer are significantly lower (both are 0.7%). (Note that 100% overlap corresponds to the two superimposed fragments.) While the design of BET-B and BET-X was focused on enhancing through-space coupling, the covalent linker also contributes to the couplings. Calculations on the model structures from which the linker was removed show a noticeable decrease in the couplings (see Figure S23 in SI). This is in line with the experimental findings for related pentacene dimers,[32] which showed that the through-bond interaction is important. The role of covalent linkers in BET-B will be quantified in future work.

Ab initio calculations were used to evaluate singlet fission rates in the selected model structures.[13,23,41] Table 1 lists the key parameters used for estimating the rate of singlet fission in the dimers. The energies used in rates calculations are defined in Computational Details. E_{sf} gives the overall thermodynamic drive for the first step, the formation of the $^1(T_1T_1)$ state. E_b is the energy difference between the pure T_1T_1 state [i.e., $^5(T_1T_1)$] and the adiabatic $^1(T_1T_1)$ state stabilized by configuration interaction; this represents a penalty for decoupling the two triplets that needs to be overcome before the triplets are separated. Figure S22 shows an energy diagram of the relevant states. The couplings between the S_1 and the $^1(T_1T_1)$ states are given by $\|\gamma\|^2$. The rates of the $^1(T_1T_1)$ formation (k_1^{rel}), and separation (k_2^{rel}), are given relative to a pair of tetracenes in a herringbone orientation.

Table 1. Energies, Couplings, And Rates of Singlet Fission Computed for the Selected Model Dimers[a]

	E_{sf} (eV)	E_b (eV)	$\|\gamma\|^2$	$\log(k_1^{rel})$	$\log(k_2^{rel})$
Tetracene	0.40	0.02	0.08	0.0	0.0
BET-B	0.03	0.15	0.04	1.9	−1.1
BET-X_1	0.45	0.07	0.17	0.1	−0.4
BET-X_2	0.36	0.04	0.12	0.3	−0.8
BET-B-excimer	0.44	0.23	0.25	0.2	−1.8
BET-X-excimer	−0.07	0.48	0.19	3.4	−3.9

[a]The rate constants here are normalized to a tetracene value of 1 for each process.

Unlike the diagram in Figure 1, the singlet fission in tetracene and in the BET-B and BET-X dimers are calculated to be endergonic, except for the BET-X excimer structure, as illustrated by Figure S22. The computed E_{sf} for tetracene is 0.40 eV. Relative to tetracene, the endergicity in BET-B is smaller. In BET-X crystal structures, E_{sf} is approximately the same as in tetracene, whereas in the BET-X excimer geometry E_{sf} becomes slightly exoergic. The lower E_{sf} of BET-B relative to tetracene is largely due to a decrease in the T_1 energy of the ET monomer versus tetracene. While the singlet energy is also lower for ET than for tetracene, there is a greater difference for the triplet energies (see SI, Table S3). The coupling of the S_0S_1 to the $^1(T_1T_1)$ state is largest for BET-X, being more than twice that of BET-B and tetracene. However, the rate of formation of the $^1(T_1T_1)$ state, which takes into account the endothermicity of singlet fission and the couplings, is predicted to be largest for BET-B. The rate of formation of $^1(T_1T_1)$ in BET-B is calculated to be roughly 2 orders of magnitude larger than for BET-X and crystalline tetracene. We have also estimated the rate of separation of $^1(T_1T_1)$ into two separated triplets, k_2. The calculations based on energetics alone (eq 2) suggest that BET-X gives a comparable rate of triplet formation from $^1(T_1T_1)$ compared to BET-B. However, in excimers the energetics of the second step are markedly different.

In the excimer calculations, we first optimized the geometry of the S_1 excimer, following the potential energy surface of the lowest state of the S_0S_1 character. We then took the optimized geometry of the excimer and carried out the calculations using the same protocol for computing the rates and parameters as for the other structures (Table 1). E_B for the BET-B excimer increases by 80 meV, whereas E_B for the BET-X excimer increases by more than 400 meV. The rate of formation of the $^1(T_1T_1)$ state from the S_1 state in the relaxed BET-B (excimer) structure is slower than that for the nonrelaxed BET-B geometry, but the opposite is seen for BET-X where this rate is 3 orders of magnitude faster for the excimer structure. In contrast, triplet formation, k_2, is markedly slower for both excimer structures relative to tetracene or their nonexcimeric structures. Thus, we suggest that the excimers might play the following role in these systems. The BET-B excimer is a weak trap, giving a k_1 nearly 2 orders of magnitude slower than the crystallographic structure for BET-B. In contrast, the BET-X excimer is a deep trap, which rapidly converts to $^1(T_1T_1)$ and is stuck there. Thus, the BET-X excimer is expected to be trapped in a $^1(T_1T_1)$ state, whereas a BET-B excimer is not expected to noticeably hinder singlet fission.

Additionally, in the excimer geometry, the coupling of the $^1(T_1T_1)$ state to the ground state of BET-X is much larger than that in BET-B ($\|\gamma\|^2 = 1.172$ and 0.014, respectively),

DOI: 10.1021/jacs.5b10550
J. Am. Chem. Soc. 2016, 138, 617−627

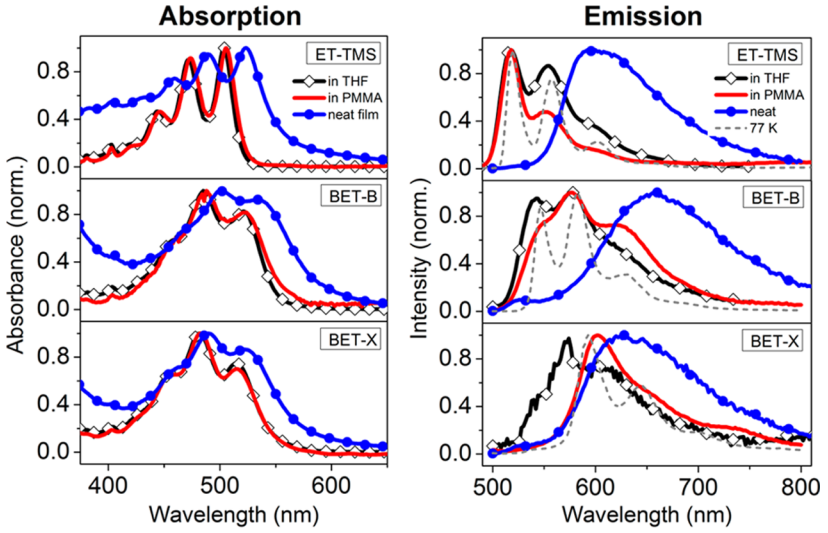

Figure 4. Absorption and emission of ET-TMS (top), BET-B (middle), and BET-X (bottom) in a THF solution (black), doped into PMMA (red), neat films (blue), and in 2-methyl-THF at 77 K (dashed gray). The intrinsic BET-X solution emission spectrum was obtained by subtracting the photooxidized impurity's emission from the measured BET-X solution emission.

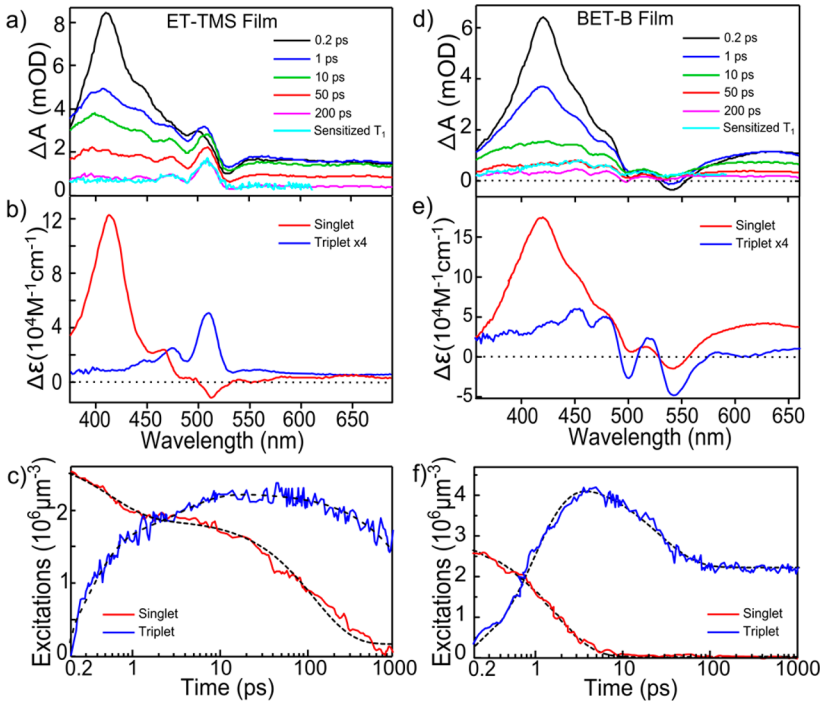

Figure 5. Transient absorption spectra of a neat film of (a) ET-TMS and (d) BET-B following excitation at 500 nm. The cyan line shows the triplet spectrum obtained from sensitization measurements of acenes with Pd(TPBP). The singlet and triplet populations for (c) ET-TMS and (f) BET-B are calculated using the extinction spectra for $S_1 \rightarrow S_n$ and $T_1 \rightarrow T_n$ transitions of (b) ET-TMS and (e) BET-B.

suggesting that the $^1(T_1T_1)$ state of BET-X will be short-lived compared to BET-B.

Photophysical Characterization. *ET-TMS.* Our photophysical studies start with the monomeric analog of the ET dimers, i.e. $(CH_3)_3Si{-}C{\equiv}C$-5-tetracene(ET-TMS). In solution, ET-TMS gives intense emission (Φ_{fl} 95%), with a 10 nm Stokes shift (Figure 4 (top)), and a lifetime of 17 ns. In a neat film, however, the emission of ET-TMS is almost entirely quenched; only a broad, featureless emission band is observed, with a significant absorption−emission energy gap of 65 nm and a quantum yield of 0.6%. The emission decay is multiexponential (SI, Figure S10), with the decay constants ranging from 22 ps (instrument resolution) to 17 ns. The source of the low-intensity, broad emission in the amorphous ET-TMS thin film is likely excimer trap sites. The absorption of the thin film is broader, and red-shifted compared to that of solution, indicating intermolecular interactions in the solid state.

Transient absorption spectra of ET-TMS in a PMMA matrix (SI, Figure S10) show an $S_1 \rightarrow S_n$ induced absorption peak at 407 nm with very little decay within 1 ns, which is consistent with the measured fluorescence lifetime (17 ns, SI, Figure S10). In a neat film of ET-TMS, however, the $S_1 \rightarrow S_n$ induced absorption signature decreases within 1 ps, and a new induced

DOI: 10.1021/jacs.5b10550
J. Am. Chem. Soc. 2016, 138, 617−627

absorption feature grows in at 510 nm (Figure 5a). Triplet sensitization measurements performed by doping a triplet sensitizer, palladium tetraphenylbenzoporphyrin (Pd(TPBP); see SI, Figure S11), confirm that the peak at 510 nm is due to the $T_1 \rightarrow T_n$ transition. The triplet yield calculations were performed using the procedure reported by Roberts et al.,[14] where the time dependent singlet and triplet populations are extracted by fitting the TA data with a linear combination of the species associated difference spectra (SADS) in extinction units for the $S_1 \rightarrow S_n$ and $T_1 \rightarrow T_n$ (Figure 5b) transitions. The extracted singlet and triplet populations (Figure 5c) give a maximum triplet yield of 90 ± 8% at only 45 ps, too fast for intersystem crossing. Efficiencies are quoted as (no. of triplets produced)/(initial no. of singlets). These experiments show that intermolecular singlet fission has occurred and the energy level criterion is fulfilled for ET-TMS; thus the $E(T_1)/E(S_1)$ ratio in BET-B and BET-X should be well positioned for them to undergo intramolecular singlet fission.

BET-B. The steady state photophysical properties of BET-B are significantly different from those of ET-TMS. The absorption of BET-B is red-shifted (18 nm, 687 cm^{-1}) relative to ET-TMS, and the absorption line shape of BET-B (Figure 4 (middle)) has an enhanced 0−1 peak and a diminished 0−0 peak. This has previously been observed in covalent dimers with cofacially oriented chromophores and attributed to Davydov interactions.[24,36,38,50] The emission intensity of BET-B in a THF solution (0.6%) and in PMMA (5.0%) is weak. The low intensity of the BET-B solution emission suggests that an excited state relaxation pathway is available in an isolated dimer, which was not present in ET-TMS. Although the BET-B Stokes shift of 23 nm has increased compared to ET-TMS, the emission line shape retains vibronic structure suggesting that emission is not due to a deep-trap excimer state. At 77 K, the methyl-THF glass solution of BET-B produces a similar emission shape to that at room temperature, but the vibronic structure is more pronounced.

The emission of an amorphous thin film of BET-B is broad and featureless, with an absorption−emission gap of 117 nm (3309 cm^{-1}). The quantum yield of the emission from a neat thin film is 0.1%. This weak emission ($\lambda_{max} \approx 650$ nm) likely originates from a small number of trap sites in the thin film of BET-B. The emission decay at 550 nm (Figure S21) further confirms that most of the singlet population (~98%) decays with an instrument limited lifetime of 22 ps. The amorphous nature of the film was confirmed by X-ray diffraction (no diffraction peaks were observed for a 66 nm thick film). In addition, a comparison of the time-resolved fluorescence decays of the amorphous thin film and single crystal of BET-B shows stark differences in the decay dynamics. Specifically, the percentage of delayed fluorescence for the crystalline BET-B is almost three times greater than the neat thin film of BET-B (SI, Figure S21). The low intensity, broad, and featureless emission from the neat film indicates that the intrinsic fluorescence of BET-B is significantly quenched in the solid state.

Unlike fluorescence spectroscopy, transient absorption captures the entire excited state population. Excitation of a thin film of BET-B at 500 nm (Figure 5d) gives an immediate ground state bleach between 475 and 575 nm, and $S_1 \rightarrow S_n$ induced absorption at 420 nm in transient absorption. The $S_1 \rightarrow S_n$ peak decreases within 1 ps, and a new structured induced absorption feature grows in at 450 nm. This new induced absorption feature is assigned to the $T_1 \rightarrow T_n$ absorption, based on the sensitization measurements of a Pd(TPBP) doped BET-B film (cyan line in Figure 5d; see SI for sensitization details). The triplet yield calculations were performed as described above for ET-TMS film, and a maximum triplet yield of 154 ± 10% at 5 ps was obtained. As illustrated in Figure 5f, the S_1 population has completely decayed in 10 ps when singlet fission is complete. This is a major difference from what was observed for ET-TMS and our previous work with DPT.[51] A second major difference is that most of the triplets generated decay rather rapidly, ~400 ps. This decrease in the $T_1 \rightarrow T_n$ absorption band is accompanied by a recovery of the ground state. This triplet lifetime is significantly shorter than that observed for the sensitized triplets (3 μs) and is independent of the excitation fluence between 8 and 4 $\mu J/cm^2$ (SI, Figure S15). These facts suggest geminate triplet−triplet annihilation to reform S_0 as the dominant triplet decay pathway in neat BET-B film.

We can now isolate the excited state dynamics to the intramolecular processes occurring in an isolated dimer by studying BET-B in dilute solution. Excitation of a THF solution of BET-B at 500 nm leads to immediate appearance of a ground state bleach between 450 and 550 nm and a familiar $S_1 \rightarrow S_n$ induced absorption band at 407 nm (Figure 6). However, with

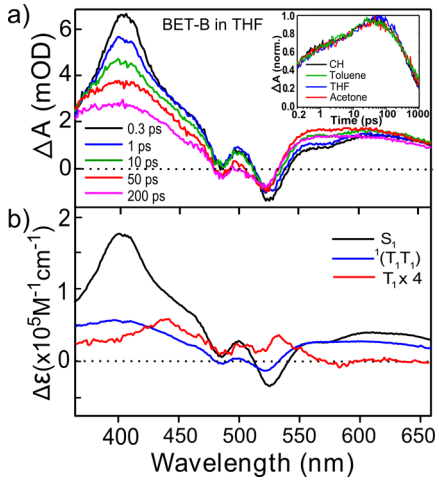

Figure 6. (a) Transient absorption spectra of BET-B in THF. The inset shows the solvent polarity independent dynamics at 560 nm for $^1(T_1T_1)$ state. (b) The comparison of spectral shape for S_1, $^1(T_1T_1)$, and T_1 state of BET-B in THF.

increasing time, the $S_1 \rightarrow S_n$ absorption decreases and a new transient state appears within 1 ps, with new induced absorption most noticeable at 560 nm, and a considerably broader absorption feature centered at ~400 nm. The transient absorption of this state does not change shape between 50 and 200 ps and does not resemble the SADS line shape associated either with BET-B $T_1 \rightarrow T_n$ or with $S_1 \rightarrow S_n$ (Figure 6b). The spectrum associated with this latter transient decays with a lifetime of 500 ps. The rate and magnitude of its formation is independent of solvent polarity and polarizability (Figure 6a, inset), ruling out a charge transfer state. Since no excimer-like steady state emission is observed in THF solution (Figure 4 (middle)), and no additional induced absorption peaks are observed in the near-IR (800−1400 nm) TA, a region generally associated with excimers,[10,52] an excimer state is ruled out as an intermediate. Instead, this transient state is assigned as the

DOI: 10.1021/jacs.5b10550
J. Am. Chem. Soc. 2016, 138, 617−627

$^1(T_1T_1)$ state (Figure 6b). Further evidence for this assignment is provided below.

The fact that fast and efficient triplet generation is observed in neat films of BET-B, but only the $^1(T_1T_1)$ state is formed in THF solution, suggests that the $^1(T_1T_1)$ state, once formed on an isolated BET-B, cannot further evolve into separated triplets, unless one of the triplets from the pair can energy transfer onto an adjacent molecule. To test this hypothesis, we doped BET-B into a film of 5,12-diphenyltetracene, DPT, a material whose T_1 energy is low enough that it can potentially accept a triplet from the $^1(T_1T_1)$ state of BET-B. The S_1 energy of DPT is higher than that of BET-B; therefore, BET-B can be selectively excited, without the possibility of singlet energy transfer. Calculations (SI, Table S3) suggest that the T_1 state of DPT (1.6 eV) is also higher than that of BET-B (1.4 eV), but triplet energy transfer is expected to be thermally accessible from the BET-B $^1(T_1T_1)$ state (2.8 eV). A sample of BET-B doped into 9,10-diphenylanthracene, DPA, was prepared as a control. Unlike DPT, the T_1 state energy of DPA is expected to be markedly higher than that of BET-B, preventing triplet transfer from BET-B to DPA. The DPA and DPT films were doped with BET-B at 26 and 17 vol %, respectively.The pump wavelength (550 nm) was chosen to avoid direct excitation of the host molecules (SI, Figure S19). BET-B doped into DPA (Figure 7a) exhibits similar transient behavior as BET-B in solution.

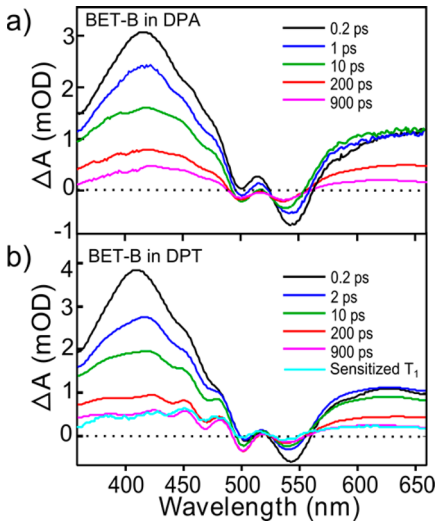

Figure 7. Transient absorption spectra of BET-B doped in (a) DPA and (b) DPT on exciting with 550 nm. The cyan line in (b) shows the triplet spectrum obtained from BET-B sensitization experiments.

Upon initial excitation to the S_1 state, the same transient $^1(T_1T_1)$ state (with induced absorption at 580 nm) is populated within 1 ps, followed by its relaxation to the ground state with a lifetime of 500 ps. Interestingly, BET-B doped into DPT (Figure 7b) initially gives similar spectral and kinetic behavior to BET-B in solution (and in DPA) up to 2 ps. At longer time delays (>10 ps), however, the distinct spectral feature for the T_1 absorption of BET-B (similar to that observed for neat BET-B film) becomes readily discernible. Simultaneously, a ground state bleach (sharp peaks at 440, 470, and 500 nm) corresponding to the DPT host emerges, suggesting triplet energy transfer from the $^1(T_1T_1)$ state of BET-B to DPT. Singlet energy transfer is ruled out, as the characteristic $S_1 \rightarrow S_n$ induced absorption for DPT is not observed[14,51] and the linear absorption spectra also suggest that the S_1 of BET-B is lower in energy than the S_1 of DPT. Thus, at longer delays the $^1(T_1T_1)$ state of BET-B relaxes to generate one T_1 (BET-B) and one T_1 (DPT) as illustrated by the simulation of TA data of BET-B in DPT film (SI, Figure S18). The combined triplet yield was found to be 120 ± 10% at 1 ns based on the extinction spectra for the $T_1 \rightarrow T_n$ transitions of BET-B and DPT. This yield calculation is a lower estimate, as the triplet transfer from the $^1(T_1T_1)$ state to one T_1 (BET-B) and one T_1 (DPT) is not fully complete within 1 ns. This slow triplet rise time is verified in the kinetic model described in the Discussion section.

BET-X. The steady state absorption spectra of BET-X (Figure 4 (bottom)) in THF solution, as well as in PMMA and neat film, are similar to those of BET-B, indicating Davydov interactions between the chromophores. Although the emission intensity of BET-X is also weak (Φ_{fl} = 2.6% in PMMA, 0.3% in neat thin film), the line shape is substantially different from that of BET-B. In all media the BET-X emission is broad and featureless, with a large gap between λ_{max} values for absorption and emission (87 nm), suggesting that BET-X undergoes emission from an excimer-like structure. In a solvent glass at 77 K, the emission still has a large energy shift, but vibrational features are apparent, indicating that the excimer-like structure is only partially formed.[53] The lifetime of the BET-X emission at 77 K is 53 ns (compared to 19 ns for ET-TMS, and 16 ns for BET-B at 77 K), supporting the excimeric nature of the emission.[54] Similar emission characteristics have been observed for an isolated, cofacially stacked pair of tetracenes at 15 K[53] and a broad featureless emission with a long lifetime was observed for cofacial anthracenes in anthracenophanes.[54,55] The emission of a neat film of BET-X is also excimer-like, but much broader and with a slightly greater red shift (106 nm) compared to the emission of BET-X in PMMA.

The transient absorption spectra of BET-X in toluene with 500 nm excitation show immediate (≤200 fs) generation of a new transient state with photoinduced absorption between 380 and 700 nm (peak at 400 nm) and ground state bleach between 450 and 550 nm [SI, Figure S20]. This transient feature is spectrally different from the $S_1 \rightarrow S_n$ induced absorption feature observed for ET-TMS and BET-B at early time (~200 fs) delays (Figure 5), but it is spectrally similar to the $^1(T_1T_1)$ induced absorption feature of BET-B [see Figure S20d]. With increasing time delay, this induced absorption feature diminishes with a concurrent ground state bleach recovery within 500 ps. During this time period, no evolution of the spectral line shape was observed in the probe window. The TA spectra of BET-X in the near-infrared (850−1400 nm) region only contain a broad red tail of the induced absorption feature between 380 and 700 nm, and no spectrally distinct peaks are observed to evolve within 1 ns. Additionally, the spectral shape and dynamics were invariable with solvent polarity and polarizability (SI, Figure S20), indicating no charge transfer state involvement in the excited state dynamics of BET-X. Attempts to measure the TA spectra of BET-X in a neat thin film and BET-X doped into DPT were unsuccessful due to photodegradation of BET-X.

DISCUSSION

We have designed an ethynyltetracene dimer (BET-B) which undergoes highly efficient intramolecular singlet fission with the production of separated triplets when in the solid state and also when doped into a host matrix with comparable T_1 energy

DOI: 10.1021/jacs.5b10550
J. Am. Chem. Soc. 2016, 138, 617−627

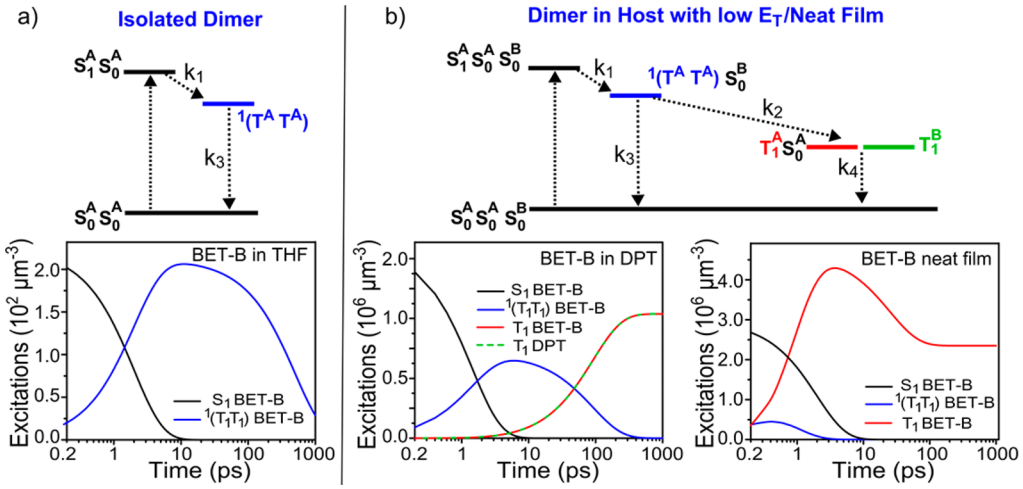

Figure 8. Kinetic model for BET-B in (a) solution, PMMA, DPA and (b) DPT, neat film. The notation A denotes the tetracenes in the same dimer, and B denotes the DPT for the BET-B in DPT film or third tetracene in another BET-B dimer for the BET-B neat film. The calculated populations for S_1 (BET-B) (black), $^1(T_1T_1)$ (BET-B) (blue), T_1 (BET-B) (red), and T_1 (DPT) (green dashed) extracted from the kinetic model are shown in the bottom panel for (a) BET-B in THF and (b) BET-B in DPT and neat BET-B film.

(DPT). Furthermore, the rates of singlet fission in amorphous ethynyltetracenes are much faster than in crystalline and polycrystalline tetracene, and amorphous films of other tetracene derivatives, such as DPT and rubrene.[14,56] The faster singlet fission rate of ethynyltetracenes is consistent with theoretical calculations, which attribute the increase in rate to a more favorable S_1 vs T_1 energy ratio in these systems compared to tetracene. Additionally, the thin film of the dimer (BET-B) produced more triplets than the thin film of the monomer (ET-TMS). This suggests that the relative orientation of the acenes found in BET-B, with the two acenes cofacially oriented at a small twisting angle, is one of the preferred orientations for singlet fission. Our TA measurements show that singlet fission takes place in neat thin films of ET-TMS and BET-B, with efficiencies of 90% and 154%, respectively. Importantly, the long diffusive singlet fission channel seen in amorphous thin films of ET-TMS and other monomeric acenes, is removed in amorphous films of the dimer, suggesting a fast, intramolecular singlet fission mechanism in the dimer film. In contrast, BET-B in solution, PMMA, and DPA thin films only proceeds to form a distinct state that is captured spectroscopically and assigned as the $^1(T_1T_1)$ state. This state is assumed to be an intermediate in triplet generation via singlet fission, but in an isolated dimer the system is trapped in this state, as the triplets are unable to separate. The $^1(T_1T_1)$ assignment is strongly supported by its observation as an intermediate followed by separation into a DPT and BET-B triplet for BET-B doped into a DPT host. The formation and decay dynamics of the $^1(T_1T_1)$ state are solvent polarity independent, indicating no significant charge transfer state involvement.

The time-dependent singlet and triplet populations extracted from the TA data of amorphous ET-TMS and BET-B thin films are shown in Figures 5c and 5f, respectively. Similarly to amorphous DPT,[14] the singlet and triplet populations in amorphous ET-TMS film exhibit both prompt and delayed excited-state dynamics. The triplet generation occurs over two time scales: a rapid exponential rise of 0.3 ps followed by a delayed power law rise stretching from 2 to 30 ps. These are assigned to a rate for singlet fission taking place directly at a preferred site close to where the exciton is initially formed and singlet fission occurring only after singlet diffusion to a preferred site, as in DPT.[14] The maximum triplet yield was found to be ~90 ± 8% at 50 ps. In contrast, the S_1 population in amorphous BET-B film decays with only a single exponential, indicating that only direct singlet fission is present with no diffusive phase adding to the singlet fission yield. Furthermore, the T_1 rise time of ~0.2 ps is faster than that in ET-TMS or DPT at the preferred sites and is comparable to the rates seen in pentacene systems.[22] Correspondingly, the maximum triplet yield in a BET-B thin film is 154 ± 10% at 5 ps. The monoexponential S_1 decay, fast T_1 rise, and high triplet yield all point toward singlet fission happening intramolecularly in amorphous BET-B. This further suggests that the intradimer preorientation in BET-B is expedient for fast singlet fission throughout the film, in contrast to amorphous monomer films where only a minority of tetracene moieties are suitably oriented.

Having formed the triplets more rapidly in BET-B films, we note that the decays of T_1 in BET-B and ET-TMS are different. ET-TMS gives a long (~2 ns) monoexponential T_1 decay, whereas in a neat BET-B film 65% of the triplets decay within 400 ps and the residual 35% remain as an offset within the 1 ns time window. This indicates that although a higher number of triplets are initially generated in a neat BET-B film, the majority of the triplets undergo geminate triplet−triplet annihilation compared to a longer lifetime for the triplets generated in the ET-TMS film, suggesting that an increase in coupling between two tetracenes increases both the formation and annihilation rates of the triplets. However, fast separation via diffusion can limit the triplet−triplet annihilation and prolong the overall triplet exciton lifetime.

Based on the TA studies of BET-B in several media, a simple scheme for the excited-state kinetics (Figure 8) is proposed where the time-dependent concentration of each transient state can be calculated by solving the coupled rate equations:

$$\frac{d[S_1]}{dt} = -k_1[S_1] \quad (3)$$

$$\frac{d[^1(T_1T_1)]}{dt} = k_1[S_1] - (k_2 + k_3)[^1(T_1T_1)] \quad (4)$$

DOI: 10.1021/jacs.5b10550
J. Am. Chem. Soc. 2016, 138, 617−627

$$\frac{d[T_1]}{dt} = 2k_2[^1(T_1T_1)] \quad (5)$$

where k_1 is the rate of formation of the $^1(T_1T_1)$ state from the S_0S_1 state, k_2 is the rate of formation of the separated triplets from the correlated triplet pair $^1(T_1T_1)$ state, and k_3 is the relaxation of the $^1(T_1T_1)$ state to the S_0 state. While time-resolved photoluminescence shows a small fraction (2−3%) of delayed fluorescence (equilibrium constant for $S_1 \rightleftarrows {}^1(T_1T_1)$ is ∼49, Figure S21), TA tracks the majority excited-state population which relaxes back to the ground state. The time-dependent concentrations obtained from solving these equations are multiplied with the corresponding SADS extinction spectra of the S_0S_1, $^1(T_1T_1)$, and T_1 states to simulate the time evolution of the TA spectra in different media. The SADS extinction spectra for these three states in different media along with the procedure to obtain them are shown in the Supporting Information (Figures S16, S17).

The TA data for BET-B in solution, PMMA, and DPA, in which only the formation of the $^1(T_1T_1)$ state is possible, were fit using Figure 8a to determine k_1 and k_3, with k_2 fixed at zero. These values are reported in Table 2. The $k_1$value is similar in all three media; however, the internal conversion rate (k_3) is slower in PMMA, due to the different density of vibronic states in solid PMMA. No separated triplets are formed in the isolated BET-B, as they cannot migrate away from one another.

Table 2. Time Constants ($\tau_i = 1/k_i$) for the Kinetic Model Used To Fit the TA Data for BET-B in Different Media

	τ_1 (ps)	τ_2 (ps)	τ_3 (±50 ps)
THF	2 ± 0.5	–	500
PMMA	1.7 ± 0.3	–	1000
DPA	2 ± 0.2	–	500
DPT	2 ± 0.3	150 ± 1	500
neat	0.8 ± 0.3	0.23 ± 0.05	500

The BET-B doped into DPT experiment illustrates the need for a third acene to give the separated triplets, i.e. T_1 (BETA) + T_1 (DPT). The selective excitation of BET-B leads to population of the S_1 state of BET-B, followed by relaxation into the $^1(T_1T_1)$ state. From 20 ps onward, distinct transient $T_1 \rightarrow T_n$ absorption spectral features of BET-B and DPT were observed. The kinetic model for singlet fission in this sample (Figure 8b) assigns two rate constants for the triplet generation process. The first rate constant (k_1) represents the conversion from S_1 to $^1(T_1T_1)$-(BET-B), while the second (k_2) represents the $^1(T_1T_1)$-(BET-B) to T_1(BET-B) + T_1(DPT) rate. These values are reported in Table 2. The k_1 and k_3 values were found to be similar to those obtained for BET-B in solution and DPA. The rate of formation (k_2) of individual triplets on BET-B and DPT from the $^1(T_1T_1)$ state was estimated to be 6.7×10^9 s^{-1} (τ_2 = 150 ps). The second rate constant (k_2) is dependent on both enthalpy and entropy. The triplet energy of DPT is slightly higher than that of BET-B (1.6 eV vs 1.4 eV), such that $^1(T_1T_1)$-(BET-B) to T_1(BET-B) + T_1(DPT) transformation is energetically uphill and the $^1(T_1T_1)$-(BET-B) state lives long enough to be experimentally detected. The driving force for this transformation is thus entropic in nature.[13,57] Assuming that each BET-B molecule is surrounded by multiple DPT molecules to which the energy transfer can occur, the entropy of the T_1(BET-B) + T_1(DPT) state is greater than that of $^1(T_1T_1)$-(BET-B), as there are several ways in which the T_1(BET-B) + T_1(DPT) state can be realized. Once the triplets, T_1(BET-B) and T_1(DPT), are generated, no relaxation was observed in the 1 ns time window.

A similar kinetic model (Figure 8b) was used to fit the TA data for the neat BET-B film. The values for k_1 and k_3 from this fit are comparable to those for BET-B in other media; however, the rate of separation to two triplets from the $^1(T_1T_1)$ state is ultrafast ($k_2 \approx 5 \times 10^{12}$ s^{-1}, $\tau_2 \approx 0.2$ ps). The faster k_2 results in rapid depopulation of the $^1(T_1T_1)$ state, such that at most only ∼10% of the $^1(T_1T_1)$ population exists at 600 fs, in the presence of 36% of the T_1(BET-B) population. As TA spectra are dominated by the $T_1 \rightarrow T_n$ absorption of BET-B, no spectral evidence for the $^1(T_1T_1)$ state was detected in the TA data for neat BET-B film. This is likely because the $^1(T_1T_1)$-(BET-B) to T_1(BET-B) + T_1(BET-B) transformation is isoenergetic or exergonic, unlike the endergonic transfer from $^1(T_1T_1)$-(BET-B) to T_1(BET-B) + T_1(DPT). Additionally, to fit the TA data for a neat BET-B film, the annihilation of the generated triplets is modeled by an initial exponential decay ($k_4 = 2.5 \times 10^9$ s^{-1}, τ_4 = 400 ps) followed by an offset to account for the long time dynamics. This fast exponential relaxation of the triplets is due to geminate triplet−triplet annihilation between the triplets present on adjacent BET-B molecules, and later when the triplets diffuse away, the recombination dynamics become slower. Irrespective of the medium, BET-B has a very fast formation rate (k_1) of the $^1(T_1T_1)$ state, indicating that the relative tetracene orientation in BET-B allows for sufficient coupling for the first step to proceed efficiently. The *ab initio* calculations corroborate the experimental results, as the formation rate for the $^1(T_1T_1)$ state in BET-B is predicted to be 2 orders of magnitude faster than in crystalline tetracene. These results suggest that the relative geometry of the acenes in BET-B is even more favorable for singlet fission than that in crystalline tetracene.

Interestingly, the transient spectral feature observed for BET-X in solution at early time delays appears to be similar to the spectral signature of the $^1(T_1T_1)$ state observed for BET-B in solution (SI, Figure S20). Based on this spectral similarity and the computed excited state energies (Figure S22) for BET-X, we posit that upon excitation in solution BET-X undergoes structural relaxation to form an excimer-like structure that may decay into the correlated triplet pair state $^1(T_1T_1)$ within 200 fs (time resolution for TA). The steady state emission of BET-X observed in rigid media could be originating from the excimer S_1 state in equilibrium with the $^1(T_1T_1)$ state, or from the $^1(T_1T_1)$ state whose wave function contains a significant admixture of the bright S_1 state (the computed oscillator strength of the $^1(T_1T_1) \rightarrow S_0$ transition at the excimer geometry of BET-X is 0.001). Since the $^1(T_1T_1)$ state in BET-X is lower in energy than that in BET-B (see SI for calculated energies) the triplet separation is expected to be markedly slower for BET-X than BET-B. Moreover, at the excimer geometry, the coupling between $^1(T_1T_1)$ and S_0 is larger for BET-X than for BET-B leading to faster decay to the ground state. Additional experiments for elucidation of the BET-X excited-state dynamics are underway.

Finally, it is important to comment on the nature of the multiexciton state, $^1(T_1T_1)$. Such a state has been identified computationally in various singlet-fission systems.[13,22,23,41,58−60] Its adiabatic wave function is dominated by the $^1(T_1T_1)$ configuration (thus, multiexciton).[41,60] However, only asymptotically this state can be described as a pure $^1(T_1T_1)$, in contrast to the $^5(T_1T_1)$ state which almost always retains pure

DOI: 10.1021/jacs.5b10550
J. Am. Chem. Soc. 2016, 138, 617−627

multiexciton character. At typical chromophore orientations, the wave function of $^1(T_1T_1)$ contains small contributions (4−6%) from other singlet configurations, such as charge-resonance (A^+B^- + A^-B^+) and excitonic (A*B + AB*) configurations.[41,60] The mixing of these configurations influences the couplings of $^1(T_1T_1)$ with the S_1 state and manifests itself in the energy splitting between the $^5(T_1T_1)$ and $^1(T_1T_1)$, E_b, and, importantly, in the optical properties of the multiexciton state. A pure multiexciton state (such as $^5(T_1T_1)$) is expected to have transient absorption spectra similar to that of a triplet, whereas the singlet multiexciton state with considerable mixing of other configurations should have a distinct spectroscopic signature, different from that of a triplet. Configuration interaction with other singlet states can also lead to intensity borrowing, which can give oscillator strength to the dark $S_0 \leftrightarrow {}^1(T_1T_1)$ transition. Although we cannot compute transient absorption spectra for the $^1(T_1T_1)$ state using the tools at our disposal, we can infer whether the multiexciton state will have different transient absorption based on the degree of mixing of other configurations. The computed E_b values (0.02−0.5 eV; see Table 1) suggest that this state features substantial contributions of the charge-resonance and excitonic configurations, which is confirmed by wave function analysis that shows the weight of the $^1(T_1T_1)$ configuration in the multiexciton state is roughly 80% and by computed oscillator strengths for the $S_0 \leftrightarrow {}^1(T_1T_1)$ transition. For example, in the X-ray structure, oscillator strengths to S_0 are 0.0004 and 0.0002 for BET-B and BET-X, respectively. In the S_1-excimer geometry, the oscillator strengths for both molecules increase to ∼0.001. Thus, we attribute the distinct transient absorption of the intermediate state to the $^1(T_1T_1)$ state, whose wave function contains significant contributions from other singlet states.

CONCLUSIONS

The excited state dynamics of the covalent tetracene dimers are highly sensitive to the relative chromophore orientation. The relative orientation of the chromophores determines the energies of the singlet, triplet, and the $^1(T_1T_1)$ states, and the couplings between those states, and, hence, the excited state relaxation pathway. In a covalent tetracene dimer in which the chromophores have a large amount of overlap (BET-X), the singlet excited state decays rapidly via either the excimer pathway or a $^1(T_1T_1)$ state trapped at the excimer-like structure from which the free triplets are no longer energetically accessible. In a covalent tetracene dimer in which the chromophores exhibit approximately one ring worth of π overlap, i.e., BET-B, the system does not relax into a deep excimer configuration. Clear evidence for a state that precedes triplet generation via singlet fission is observed. We assign this as the $^1(T_1T_1)$ or the multiexciton state. In BET-B, without forming a strongly bound excimer, the tetracenes possess sufficient orbital overlap to couple the S_0S_1 and $^1(T_1T_1)$ states and to promote rapid conversion of S_0S_1 to $^1(T_1T_1)$.

In the tetracene systems, singlet fission is slightly endothermic; therefore, the entropy gain on producing the separated triplets by singlet fission plays a key role. Once the $^1(T_1T_1)$ state is formed in an isolated dimer (BET-B), the system cannot separate the correlated triplets, and the state decays to the ground state by radiationless relaxation. However, when BET-B is placed into a tetracene-rich matrix comprised of DPT or other BET-B molecules, triplets efficiently transfer from $^1(T_1T_1)$ to the host. Therefore, for systems in which singlet fission is endothermic, the triplet energy transfer is an essential second step required for the production of free triplet excitons.

Covalent dimers hold promise for exploiting singlet fission in photovoltaic materials. We have observed ultrafast, efficient, intramolecular singlet fission in a neat amorphous film of BET-B. The triplet yield in the neat film of the dimer, BET-B, is 154 ± 10%, while the neat film of the monomer analog, ET-TMS, produces triplets with only 90 ± 8% efficiency. The elimination of a diffusive phase in the singlet fission kinetics suggests that by preorienting all chromophores into a preferred singlet fission geometry, we can increase the singlet fission efficiency in disordered materials. This will relax the constraints placed on the film manufacturing process to achieve low-cost, high efficiency singlet fission based OPVs.

ASSOCIATED CONTENT

Supporting Information

The Supporting Information is available free of charge on the ACS Publications website at DOI: 10.1021/jacs.5b10550.

The synthetic details, structural characterization of the materials, additional computational data, details of the triplet yield calculations, detailed sample preparation, extinction spectra, triplet sensitization spectra and detailed kinetic analysis (PDF)
Crystallgraphic data for BET-B (CIF)
Crystallgraphic data for BET-X (CIF)

AUTHOR INFORMATION

Corresponding Authors

*stephen.bradforth@usc.edu
*met@usc.edu

Author Contributions

‡N.V.K. and S.D. contributed equally.

Notes

The authors declare the following competing financial interest(s): Mark Thompson has a financial interest in Nanoflex Power Corporation.

ACKNOWLEDGMENTS

We thank Prof. John Spence for providing BEA-B, Ms. Kelsey Bass for thin-film X-ray diffraction measurements, Prof. David Casanova for his help with wave function analysis, and Prof. Peter Djurovich for fruitful discussions. M.E.T. and N.V.K. acknowledge support from Nanoflex Power Corporation. A.I.K. acknowledges support from the U.S. Department of Energy, Office of Science, Office of Basic Energy Sciences, through Grant No. DE-FG02-05ER15685 and through the Scientific Discovery through Advanced Computing (SciDAC) program. S.E.B. and S.D. acknowledge support from the Center for Energy Nanoscience, an Energy Frontier Research Center funded by the U.S. Department of Energy, Office of Science, Office of Basic Energy Sciences (DE-SC0001013).

REFERENCES

(1) Shockley, W.; Queisser, H. J. *J. Appl. Phys.* **1961**, *32*, 510−519.
(2) Smith, M. B.; Michl, J. *Chem. Rev.* **2010**, *110*, 6891−6936.
(3) Grumstrup, E. M.; Johnson, J. C.; Damrauer, N. H. *Phys. Rev. Lett.* **2010**, *105*, 257403.
(4) Wang, C.; Schlamadinger, D. E.; Desai, V.; Tauber, M. J. *ChemPhysChem* **2011**, *12*, 2891−11833.

DOI: 10.1021/jacs.5b10550
J. Am. Chem. Soc. 2016, 138, 617−627

(5) Johnson, J. C.; Nozik, A. J.; Michl, J. *Acc. Chem. Res.* **2013**, *46*, 1290−1299.
(6) Burdett, J. J.; Bardeen, C. J. *Acc. Chem. Res.* **2013**, *46*, 1312−1320.
(7) Wilson, M. W.; Rao, A.; Clark, J.; Kumar, R. S. S.; Brida, D.; Cerullo, G.; Friend, R. H. *J. Am. Chem. Soc.* **2011**, *133*, 11830−11833.
(8) Burdett, J. J.; Müller, A. M.; Gosztola, D.; Bardeen, C. J. *J. Chem. Phys.* **2010**, *133*, 144506.
(9) Chan, W.-L.; Ligges, M.; Jailaubekov, A.; Kaake, L.; Miaja-Avila, L.; Zhu, X.-Y. *Science* **2011**, *334*, 1541−1545.
(10) Stern, H. L.; Musser, A. J.; Gelinas, S.; Parkinson, P.; Herz, L. M.; Bruzek, M. J.; Anthony, J.; Friend, R. H.; Walker, B. J. *Proc. Natl. Acad. Sci. U. S. A.* **2015**, *112*, 7656−7661.
(11) Walker, B. J.; Musser, A. J.; Beljonne, D.; Friend, R. H. *Nat. Chem.* **2013**, *5*, 1019−1024.
(12) Chan, W.-L.; Ligges, M.; Zhu, X. *Nat. Chem.* **2012**, *4*, 840−845.
(13) Kolomeisky, A. B.; Feng, X.; Krylov, A. I. *J. Phys. Chem. C* **2014**, *118*, 5188−5195.
(14) Roberts, S. T.; McAnally, R. E.; Mastron, J. N.; Webber, D. H.; Whited, M. T.; Brutchey, R. L.; Thompson, M. E.; Bradforth, S. E. *J. Am. Chem. Soc.* **2012**, *134*, 6388−6400.
(15) Smith, M. B.; Michl, J. *Annu. Rev. Phys. Chem.* **2013**, *64*, 361−386.
(16) Akdag, A.; Havlas, Z. k.; Michl, J. *J. Am. Chem. Soc.* **2012**, *134*, 14624−14631.
(17) Ryerson, J. L.; Schrauben, J. N.; Ferguson, A. J.; Sahoo, S. C.; Naumov, P. e.; Havlas, Z. k.; Michl, J.; Nozik, A. J.; Johnson, J. C. *J. Phys. Chem. C* **2014**, *118*, 12121−12132.
(18) Thorsmølle, V. K.; Averitt, R. D.; Demsar, J.; Smith, D.; Tretiak, S.; Martin, R.; Chi, X.; Crone, B.; Ramirez, A.; Taylor, A. *Phys. Rev. Lett.* **2009**, *102*, 017401.
(19) Zhang, B.; Zhang, C.; Xu, Y.; Wang, R.; He, B.; Liu, Y.; Zhang, S.; Wang, X.; Xiao, M. *J. Chem. Phys.* **2014**, *141*, 244303.
(20) Birech, Z.; Schwoerer, M.; Schmeiler, T.; Pflaum, J.; Schwoerer, H. *J. Chem. Phys.* **2014**, *140*, 114501.
(21) Piland, G. B.; Bardeen, C. J. *J. Phys. Chem. Lett.* **2015**, *6*, 1841−1846.
(22) Yost, S. R.; Lee, J.; Wilson, M. W.; Wu, T.; McMahon, D. P.; Parkhurst, R. R.; Thompson, N. J.; Congreve, D. N.; Rao, A.; Johnson, K. *Nat. Chem.* **2014**, *6*, 492−497.
(23) Feng, X.; Kolomeisky, A. B.; Krylov, A. I. *J. Phys. Chem. C* **2014**, *118*, 19608−19617.
(24) Margulies, E. A.; Shoer, L. E.; Eaton, S. W.; Wasielewski, M. R. *Phys. Chem. Chem. Phys.* **2014**, *16*, 23735−23742.
(25) Mataga, N.; Yao, H.; Okada, T.; Rettig, W. *J. Phys. Chem.* **1989**, *93*, 3383−3386.
(26) Kolata, K.; Breuer, T.; Witte, G.; Chatterjee, S. *ACS Nano* **2014**, *8*, 7377−7383.
(27) Marciniak, H.; Fiebig, M.; Huth, M.; Schiefer, S.; Nickel, B.; Selmaier, F.; Lochbrunner, S. *Phys. Rev. Lett.* **2007**, *99*, 176402.
(28) Marciniak, H.; Pugliesi, I.; Nickel, B.; Lochbrunner, S. *Phys. Rev. B: Condens. Matter Mater. Phys.* **2009**, *79*, 235318.
(29) Müller, A. M.; Avlasevich, Y. S.; Müllen, K.; Bardeen, C. J. *Chem. Phys. Lett.* **2006**, *421*, 518−522.
(30) Müller, A. M.; Avlasevich, Y. S.; Schoeller, W. W.; Müllen, K.; Bardeen, C. J. *J. Am. Chem. Soc.* **2007**, *129*, 14240−14250.
(31) Johnson, J. C.; Akdag, A.; Zamadar, M.; Chen, X.; Schwerin, A. F.; Paci, I.; Smith, M. B.; Havlas, Z.; Miller, J. R.; Ratner, M. A. *J. Phys. Chem. B* **2013**, *117*, 4680−4695.
(32) Zirzlmeier, J.; Lehnherr, D.; Coto, P. B.; Chernick, E. T.; Casillas, R.; Basel, B. S.; Thoss, M.; Tykwinski, R. R.; Guldi, D. M. *Proc. Natl. Acad. Sci. U. S. A.* **2015**, *112*, 5325−5330.
(33) Busby, E.; Xia, J.; Wu, Q.; Low, J. Z.; Song, R.; Miller, J. R.; Zhu, X.; Campos, L. M.; Sfeir, M. Y. *Nat. Mater.* **2015**, *14*, 426−433.
(34) Sanders, S. N.; Kumarasamy, E.; Pun, A. B.; Trinh, M. T.; Choi, B.; Xia, J.; Taffet, E. J.; Low, J. Z.; Miller, J. R.; Roy, X.; Zhu, X. Y.; Steigerwald, M. L.; Sfeir, M. Y.; Campos, L. M. *J. Am. Chem. Soc.* **2015**, *137*, 8965−8972.
(35) Busby, E.; Xia, J.; Low, J. Z.; Wu, Q.; Hoy, J.; Campos, L. M.; Sfeir, M. Y. *J. Phys. Chem. B* **2015**, *119*, 7644−7650.
(36) Lindquist, R. J.; Lefler, K. M.; Brown, K. E.; Dyar, S. M.; Margulies, E. A.; Young, R. M.; Wasielewski, M. R. *J. Am. Chem. Soc.* **2014**, *136*, 14912−14923.
(37) Giaimo, J. M.; Lockard, J. V.; Sinks, L. E.; Scott, A. M.; Wilson, T. M.; Wasielewski, M. R. *J. Phys. Chem. A* **2008**, *112*, 2322−2330.
(38) Liu, H.; Nichols, V. M.; Shen, L.; Jahansouz, S.; Chen, Y.; Hanson, K. M.; Bardeen, C. J.; Li, X. *Phys. Chem. Chem. Phys.* **2015**, *17*, 6523−6531.
(39) Johnson, J. M.; Chen, R.; Chen, X.; Moskun, A. C.; Zhang, X.; Hogen-Esch, T. E.; Bradforth, S. E. *J. Phys. Chem. B* **2008**, *112*, 16367−16381.
(40) Shao, Y.; Gan, Z.; Epifanovsky, E.; Gilbert, A. T.; Wormit, M.; Kussmann, J.; Lange, A. W.; Behn, A.; Deng, J.; Feng, X. *Mol. Phys.* **2015**, *113*, 184−215.
(41) Feng, X.; Luzanov, A. V.; Krylov, A. I. *J. Phys. Chem. Lett.* **2013**, *4*, 3845−3852.
(42) Casanova, D.; Slipchenko, L. V.; Krylov, A. I.; Head-Gordon, M. *J. Chem. Phys.* **2009**, *130*, 044103.
(43) Bell, F.; Zimmerman, P. M.; Casanova, D.; Goldey, M.; Head-Gordon, M. *Phys. Chem. Chem. Phys.* **2013**, *15*, 358−366.
(44) Casanova, D.; Head-Gordon, M. *Phys. Chem. Chem. Phys.* **2009**, *11*, 9779−9790.
(45) Korovina, N. V.; Chang, M. L.; Nguyen, T. T.; Fernandez, R.; Walker, H. J.; Olmstead, M. M.; Gherman, B. F.; Spence, J. D. *Org. Lett.* **2011**, *13*, 3660−3663.
(46) Chen, Z.; Müller, P.; Swager, T. M. *Org. Lett.* **2006**, *8*, 273−276.
(47) Chi, X.; Li, D.; Zhang, H.; Chen, Y.; Garcia, V.; Garcia, C.; Siegrist, T. *Org. Electron.* **2008**, *9*, 234−240.
(48) Moon, H.; Zeis, R.; Borkent, E.-J.; Besnard, C.; Lovinger, A. J.; Siegrist, T.; Kloc, C.; Bao, Z. *J. Am. Chem. Soc.* **2004**, *126*, 15322−15323.
(49) Schmidt, R.; Gottling, S.; Leusser, D.; Stalke, D.; Krause, A.-M.; Wurthner, F. *J. Mater. Chem.* **2006**, *16*, 3708−3714.
(50) Veldman, D.; Chopin, S. M.; Meskers, S. C.; Groeneveld, M. M.; Williams, R. M.; Janssen, R. A. *J. Phys. Chem. A* **2008**, *112*, 5846−5857.
(51) Roberts, S. T.; McAnally, R. E.; Mastron, J. N.; Webber, D. H.; Whited, M. T.; Brutchey, R. L.; Thompson, M. E.; Bradforth, S. E. *J. Am. Chem. Soc.* **2012**, *134*, 6388−6400.
(52) Diri, K.; Krylov, A. I. *J. Phys. Chem. A* **2012**, *116*, 653−662.
(53) Iannone, M. A.; Scott, G. W. *Chem. Phys. Lett.* **1990**, *171*, 569−574.
(54) Morita, M.; Kishi, T.; Tanaka, M.; Tanaka, J.; Ferguson, J.; Sakata, Y.; Misumi, S.; Hayashi, T.; Mataga, N. *Bull. Chem. Soc. Jpn.* **1978**, *51*, 3449−3457.
(55) Neelakandan, P. P.; Sanju, K. S.; Ramaiah, D. *Photochem. Photobiol.* **2010**, *86*, 282−289.
(56) Piland, G. B.; Burdett, J. J.; Kurunthu, D.; Bardeen, C. J. *J. Phys. Chem. C* **2013**, *117*, 1224−1236.
(57) Chan, W.-L.; Ligges, M.; Zhu, X.-Y. *Nat. Chem.* **2012**, *4*, 840−845.
(58) Zimmerman, P. M.; Zhang, Z.; Musgrave, C. B. *Nat. Chem.* **2010**, *2*, 648−652.
(59) Zimmerman, P. M.; Bell, F.; Casanova, D.; Head-Gordon, M. *J. Am. Chem. Soc.* **2011**, *133*, 19944−19952.
(60) Luzanov, A. V.; Casanova, D.; Feng, X.; Krylov, A. I. *J. Chem. Phys.* **2015**, *142*, 224104.

DOI: 10.1021/jacs.5b10550
J. Am. Chem. Soc. 2016, 138, 617−627